Clinical and Experimental Medicine (2026) 26:231
https://doi.org/10.1007/s10238-026-02188-2

RESEARCH

Single-cell atlas reveals the key role of pro-inflammatory IREB2⁺ microglia subsets in the microenvironment of Alzheimer's disease

Wenzheng Rong[1,2,3] · Jing Xu[4] · Bo Li[1,3] · Yapeng Li[1,2,3] · Yuming Xu[1,2,3]

Received: 4 April 2026 / Accepted: 9 May 2026

Abstract

Chronic neuroinflammation driven by activated microglia is a critical hallmark of Alzheimer's disease (AD) progression. Metabolic dysregulation, particularly iron metabolism, has been implicated in neurodegeneration, yet the role of iron-responsive element-binding protein 2 (IREB2) in AD-associated neuroinflammation remains poorly understood. We performed integrative analysis of single-cell RNA sequencing (scRNA-seq) data from AD brain tissues, using non-negative matrix factorization (NMF) and intercellular communication algorithms to map cellular landscapes. We identified microglial subpopulations and their inflammatory signaling. To experimentally validate the functional role of IREB2 in inflammatory responses, we conducted siRNA-mediated knockdown in the human neuroblastoma cell line SH-SY5Y, which serves as a neuronal model for assessing IREB2's effect on cytokine expression. Single-cell analysis revealed a distinct microglial subpopulation (IREB2⁺ MC C1) that is significantly expanded in AD. This subpopulation exhibits a hyper-inflammatory state, with enrichment of Toll-like receptor and IL-17 signaling pathways, and functions as a primary source of outgoing inflammatory signals (CCL3, CCL4). Furthermore, IREB2 knockdown in SH-SY5Y cells significantly suppressed the expression of key pro-inflammatory cytokines (IL6, IL-1β, and TNF-α), confirming that IREB2 positively regulates inflammation in neurons as well. IREB2 drives both microglial activation and neuronal inflammatory responses in AD, potentially via the NF-κB pathway. The IREB2⁺ microglial subpopulation represents a specific pathogenic entity that orchestrates the inflammatory microenvironment. Targeting IREB2 may therefore offer a dual-pronged therapeutic strategy to mitigate neuroinflammation and slow AD progression.

Keywords Alzheimer's disease · IREB2 · Neuro-inflammation · IL-6 · TNF-a · IL-6

Introduction

Alzheimer's disease (AD) is the most common form of dementia worldwide and it appears with degenerating cognitive functions as well as with the formation of amyloid-β deposits and neurofibrillary clusters [1–5]. Currently, there are no highly effective therapeutic interventions. There is accumulating evidences that neuroinflammatory processes are involved in the development of the AD, where the reactive microglial cells and also the astroglia are important in the impairment of the synaptic activity and the nerve cell death [6–10]. However, the big diversity of the inflammatory mechanisms in the brains of the AD affected, remains to be elucidated.

Cutting-edge developments in single-cell transcriptomic analysis (scRNA-seq) have enabled us to map the very different cellular composition in neurodegenerative conditions [11–15]. Through this technology, specialized microglial

Wenzheng Rong and Jing Xu contributed equally to this work.

✉ Yuming Xu
xuyuming@zzu.edu.cn

1 Department of Neurology, The First Affiliated Hospital of Zhengzhou University, Zhengzhou University, Zhengzhou, Henan, People's Republic of China

2 Tianjian Laboratory of Advanced Biomedical Sciences, School of life sciences, Zhengzhou University, Zhengzhou, Henan, China

3 NHC Key Laboratory of Prevention and Treatment of Cerebrovascular Diseases, Henan Key Laboratory of Cerebrovascular Diseases, Zhengzhou, Japan

4 Department of Endocrinology, The First Affiliated Hospital of Zhengzhou University, Zhengzhou, China

Published online: 20 May 2026

populations related to the pathology (DAM) or activated astrocyte phenotypes as well as disrupted cell to cell signaling pathways have been unveiled. The exact gene regulatory networks that link the metabolic dysfunction, the oxidative damage and pro-inflammatory cascades that take place in different neural cell types are not well characterized [16–20]. One of the most interesting is ferroptosis - a particular type of cell death mediated by the iron accumulated and the lipid oxidation that have strong links with the neuroinflammation. This pathway has appeared as potential important in the path of Alzheimer's disease, but if ferroptosis related transcriptional patterns exist and are functionally relevant in some kind of macrophage/microglial populations in the brain of AD is to be explored.

Other important proteins in which also have been related with fat processing and stimulation of immune cells in non neural tissues like for example IREB2 [21]. Nevertheless, their different cellular distribution and the role in the inflammation of the brain related to AD are not studied yet. In the same way the molecular signaling systems that control the communication between different kind of cells in the brain (glial cells, blood vessel cells and neurons) in the inflammatory environment of AD also need to be more studied.

Materials and methods

Single-cell multi-omics progression analysis

We used Seurat software to make the Seurat objects of data analysis. The dataset GSE188545 is downloaded from the Gene Expression Omnibus repository (https://www.ncbi.nlm.nih.gov/geo/). Six biological specimens were used for the following investigation according to the 10× Genomics single-cell RNA sequencing protocol. We implement the Seurat 4.0 R toolkit to build a unified Seurat object with all experimental samples. In the quality control procedures, we only kept cells that expressed between 200 and 4000 genes, and kept the expression of the mitochondrial gene is under 10% of total cellular transcripts [22–25].

Data normalization and dimensionality reduction

We have normalized and performed the variance stability with the SCTransform approach in Seurat of the dataset, taking into account the mitochondrial gene content and the total numbers of UMI. We have done the linear dimensionality reduction by doing the principal component analysis (PCA) on the genes with high variability, and we have choose the first 30 of principal components to look at them. We have mapped the cellular relationships by doing the FindNeighbors algorithm, and we have found the cluster by doing the FindClusters method (with the cluster resolution set to 0.5). For the spatial representation, we have generated two dimensional projections with the uniform manifold approximation and projection (UMAP).

Differential expression and functional enrichment analysis

The variations of the gene expression that separate AD samples from healthy control (HC) samples, and the one between the different cellular subtypes were found using the FindMarkers tool of Seurat. We set the criterium of statistical significance with the absolute value of the log2 fold change bigger than 0.25 and the Bonferroni adjusted p value smaller than 0.05. Then, we used clusterProfiler version 4.0 (R software package) to do the KEGG pathway analysis and Gene Ontology annotation of these found genes. The enrichment result was considered significant when the corrected p value was less than 0.05.

Single-cell functional scoring

We used three different computational ways (AUCell, UCell and singscore) to measure the activity level of the defined gene collections in the single cells. The gene collections were taken from the MSigDB repository (inflammation related pathways, oxidative stress related markers, metabolic processes) or were manually defined (ferroptosis related genes).

AUCell found enrichment by evaluating the area of the integral of the curve, UCell used a ranking based statistical method. With the singscore, the quantitative assessments have come from the rank normalisation procedures. These three independent measurement were finally average to get the composite functional activity index .

NMF subpopulation analysis

To identify hidden cellular subpopulations, we applied non-negative matrix factorization (NMF) to the expression matrix of microglial cells (selected from the global clustering). The gene expression matrix X (cells × genes) was factorized into two non-negative matrices: W (cells × k) representing cell-factor loadings, and H (k × genes) representing factor-gene weights. Factorization was performed using the NMF R package (method = "brunet", rank k ranging from 2 to 15) with 100 iterations to ensure stability. The optimal rank k was selected based on the cophenetic correlation coefficient and the average silhouette width.

To assign cells into discrete subpopulations, we performed consensus k-means clustering on the W matrix (cell-factor loading matrix) using Euclidean distance and

100 random initializations. The number of clusters was set equal to the optimal NMF rank k. The robustness of clustering was assessed by bootstrap resampling (80% of cells, 200 iterations). For each resulting subpopulation, the characteristic factor genes were defined as those with the highest loading scores in the corresponding row of H (top 50 genes per factor). These gene signatures were then used for pathway enrichment analysis (GO, KEGG) and to annotate the biological identity of each subpopulation, such as the $IREB2^{+}$ hyper-inflammatory microglial cluster (MC C1).

Cell–cell communication analysis

Cell-cell communication was analyzed using CellPhoneDB v5.0. To exclude false positive signals caused by low or random expression, the single-cell expression matrix was pre-filtered: only genes detected in at least 10% of cells within a given cell type (expression proportion > 10%) were retained. On this basis, we further required that both genes in a ligand-receptor pair have an average expression level greater than 0.5 (after log1p normalization) or 1 (raw UMI count) in the respective cell types, thereby removing low-expression interactions with limited biological significance. Additionally, a "ligand-receptor co-expression" strategy was adopted to screen for high-confidence interactions: a ligand-receptor pair was included only if the proportion of cells expressing the ligand in the sender cell type and the proportion of cells expressing the receptor in the receiver cell type both exceeded 10%, and the geometric mean of their expression abundances was higher than the median of the global background distribution. These thresholds were determined empirically based on data distribution characteristics to balance sensitivity and specificity.

Cell culture

The SH-SY5Y and BV2 cell line was purchased from Type Culture Collection of Chinese Academy of Sciences, Shanghai. The cells were cultured in DMEM/F12 growth medium (Gibco, USA) supplemented with 10% fetal bovine serum (FBS, Gibco, USA) and 1% penicillin-streptomycin solution (Beyotime, China), and maintained at 37, 5% CO_2 in humid atmosphere. In the gene silencing experiments, 50 nM of IREB2-targeting small interfering RNA (si-IREB2) or non-targeting control siRNA (si-NC) (GenePharma, Shanghai) were introduced into the cells by Lipofectamine 3000 transfection reagent (Invitrogen, USA) according to the supplier's protocol. And the cellular samples were collected after 48 h of transfection for the further test .

RNA Extraction and Quantitative Real-Time PCR

The cellular RNA was isolated with TRIzol solution (Invitrogen, USA) in strict accordance with the supplier instructions. The RNA quality was assessed by the absorbance measurements at 260 nm and 280 nm wavelengths with the NanoDrop spectrophotometric device (Thermo Scientific, USA). The reverse transcription was done with 1 g of isolated RNA with the PrimeScript RT Reagent Kit containing gDNA Eraser (Takara, Japan). The quantitative PCR analysis was done on a CFX96 Touch Real-Time PCR instrument (Bio-Rad, USA) with the TB Green Premix Ex Taq reagents (Takara, Japan). PCR protocol was as follows, an initial denaturation at 95 for 30s, followed by 40 amplification cycles of 5s denaturation at 95 and 30s annealing/extension at 60. IREB2 transcript levels were normalised to GAPDH and were quantified by the comparative Ct (2^(-ΔΔCt)) approach.

Enzyme-linked immunosorbent assay

The levels of important inflammatory mediators, such as IL-1β, IL-6 and TNF- α, which are present in the cell culture supernatants, were quantified with the enzyme-linked immunosorbent assay (ELISA) using standard commercial kits (MultiSciences, China). According to the producer protocol, 100 mL aliquots of either the standard solutions or the experimental samples were added into the antibody precoated 96-well plates and kept at the 37 C for a 2 h incubation. After three thorough washes with the defined buffer solution, each well was put into 100 mL of enzyme-linked detection reagent and was incubated for 60 min at the same temperature. After another washing, 100 mL of chromogenic substrate was dispensed into all wells and was allowed to develop for 30 min at the 37 C, in the light protected condition. The enzymatic reaction was stopped by the introduction of 100 mL of stop solution and the absorbance readings at the 450 nm wavelength was obtained with a microplate absorbance reader (BioTek, USA). The final cytokine quantities were obtained through the interpolation of the standard calibration curve and then adjusted by the total protein measurements.

Statistical analysis

Each experimental procedure was done with three replicates and repeated independent three times. The results are shown as averages with the standard deviation values. For the statistical difference between two sample groups, an unpaired Student's t-test was used using GraphPad Prism 9.0 software.

Results

Single-cell transcriptomic profiling uncovers modified cell population dynamics in AD brain tissue

We have performed single-cell transcriptomic profiling of brain tissue samples that were obtained postmortem, in order to look at the cellular diversity associated to AD. With the help of dimensionality reduction techniques (UMAP), we were able to see clear segregation of principal neural cell populations, like neuronal cells, astroglial cells, microglial cells, oligodendroglial cells, and vascular endothelial cells (Fig. 1A). Transcriptional profiles from the specimens of AD are seen to have substantial divergence from that of the neurologically normal, and we can see alterations in the cellular clustering (Fig. 1B). Quantitatively, the changes of the cell population (Fig. 1D), there is a large increase of the microglia that are showing the disease associated phenotypes (DAM) and activated astrocytes and some of the neuronal subtypes are clearly depleted, which shows the large cellular reorganization that is taking place in AD pathogenesis.

Metabolic-inflammatory reprogramming characterizes AD cell subpopulations

In order to evaluate the functional characteristics of these transformed cells, we have performed in detail the cell type classification and pathway enrichment analysis with the use of different scoring (AUCell, UCell, singscore). We showed that in the case of the Alzheimer's disease we have investigated there is a disease specific transition towards the pro-inflammatory and metabolic dysfunction profiles (Fig. 2B). In particular, the activation of the immune related pathways and the markers of redox imbalance are the most pronounced in glial cells. We also detected a cluster of the immune-associated marker genes with high expression level in the cases of AD, which contains the modulators of the lipid homeostasis (ACSL1, MACH1) and mediators of the cellular stress (SERPINF1) (Fig. 2E). These observations reveal the coordinated disturbances of the metabolic-immune crosstalk and of the inflammatory pathways among different neural cell populations in the AD pathology.

Transcriptional dynamics identify dysregulated iron and lipid metabolism in AD

A systematic comparison of the transcriptional pattern of AD patients vs. HC showed many genes with differential expression (Fig. 3A). The functional pathway analysis showed strong modifications in the biological processes related to the iron homeostasis (among others FTH1 and STEAP3) and cellular defense against oxidative damage (among others SAT1 and HSP90) suggesting a global metabolic restructuration in the neural tissue of AD patients. Different cellular groups (especially Clusters 10, 13 and 18) shown remarkable reorganization pattern in AD cases (Fig. 3B) suggesting the development of specific inflammatory cellular phenotypes. The flow cytometry analysis showed the fluctuating proportion in the cell subsets related to the inflammation (Gate 3 and Gate 8), which pave the way to find particular metabolic-inflammatory paths related to the iron regulation and lipid metabolism.

Fig. 1 Single-cell RNA sequencing comprehensive analysis of cellular diversity in human brain specimens. (**A**) Two-dimensional UMAP visualization of cells from all samples after unsupervised clustering of 22 individual cellular clusters (labeled 0–21). Individual cells are shown by the colored dot corresponding to the assigned cluster. (**B-G**) Matrix plots of the proportion of cells from different experimental batches and clinical conditions (healthy, tumorous) in each of the identified cluster. These visualizations show that the cellular populations are coming from several sources without strong technical artefacts or segregation of the popualtions in a disease specific way. (**H**) Classification of the 22 clusters in the UMAP projection with cell-type specific molecular markers, and their organization in 7 principal cellular categories: Oligodendrocytes, Inhibitory_Neurons, Excitatory_Neurons, Astrocytes, Microglial cells, and Vascular Endothelial cells. (**I**) examination of atlas cellular distribution. The left histogram gives the total of the cells identified for each of the 7 major

Intercellular crosstalk highlight metabolic vulnerability

As the abundance of the metabolic genes considered in AD is increased, we also considered the spatial distribution of the expression of ACSL1 (Acyl-CoA Synthetase Long-Chain Family Member 1) which is accumulated in both endothelial cells and microglial cells (Fig. 4A-B). This means that they are importantly involved in the impaired lipid metabolism. Considering the ligand-receptor interaction studies (Fig. 4F) we have seen the strengthened of the signalings associated with ACSL1, in particular the VEGFA-VEGFR1 and TGFB2-TGFBR systems, which show some dynamic metabolic-inflammatory interaction. The fact that in particular some cell clusters the genes that regulate the lipid metabolism and the iron homeostasis (including IREB2) are at the same time present, make us to think of the ferroptosis as a possible medidor of this kind of cell communication.

IREB2-defined macrophage subpopulation exhibits pro-inflammatory metabolic features

In order to deal with the diversity that we saw for macrophages and microglia, we did a subclustering analysis with non-negative matrix factorization (NMF) with the

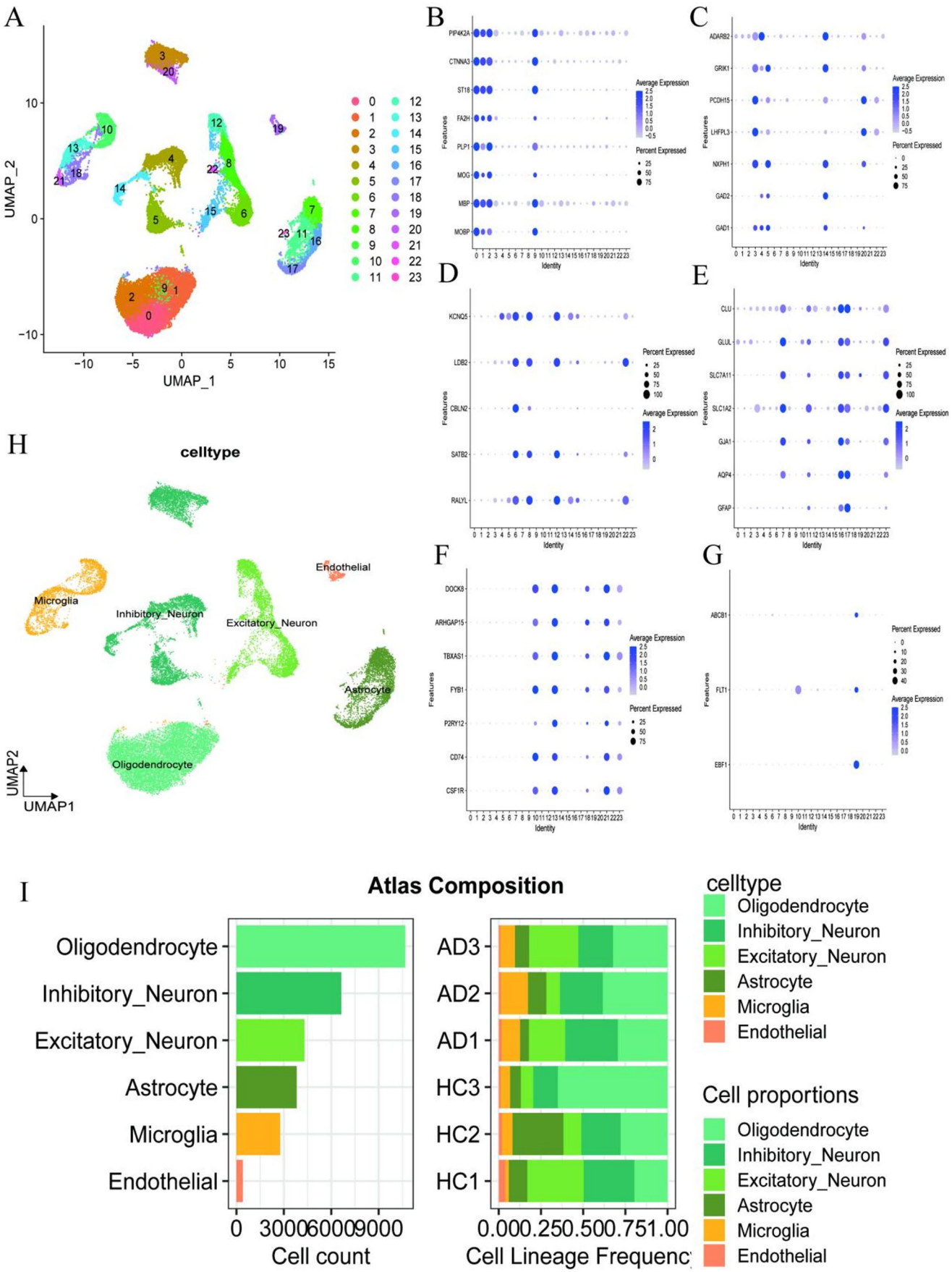
A
UMAP_2
UMAP_1
B
C
D
E
F
G
H
celltype
Endothelial
Microglia
Inhibitory_Neuron
Excitatory_Neuron
Astrocyte
Oligodendrocyte
UMAP2
UMAP1
I
Atlas Composition
Oligodendrocyte
Inhibitory_Neuron
Excitatory_Neuron
Astrocyte
Microglia
Endothelial
Cell count
AD3
AD2
AD1
HC3
HC2
HC1
Cell Lineage Frequenc
celltype
Cell proportions

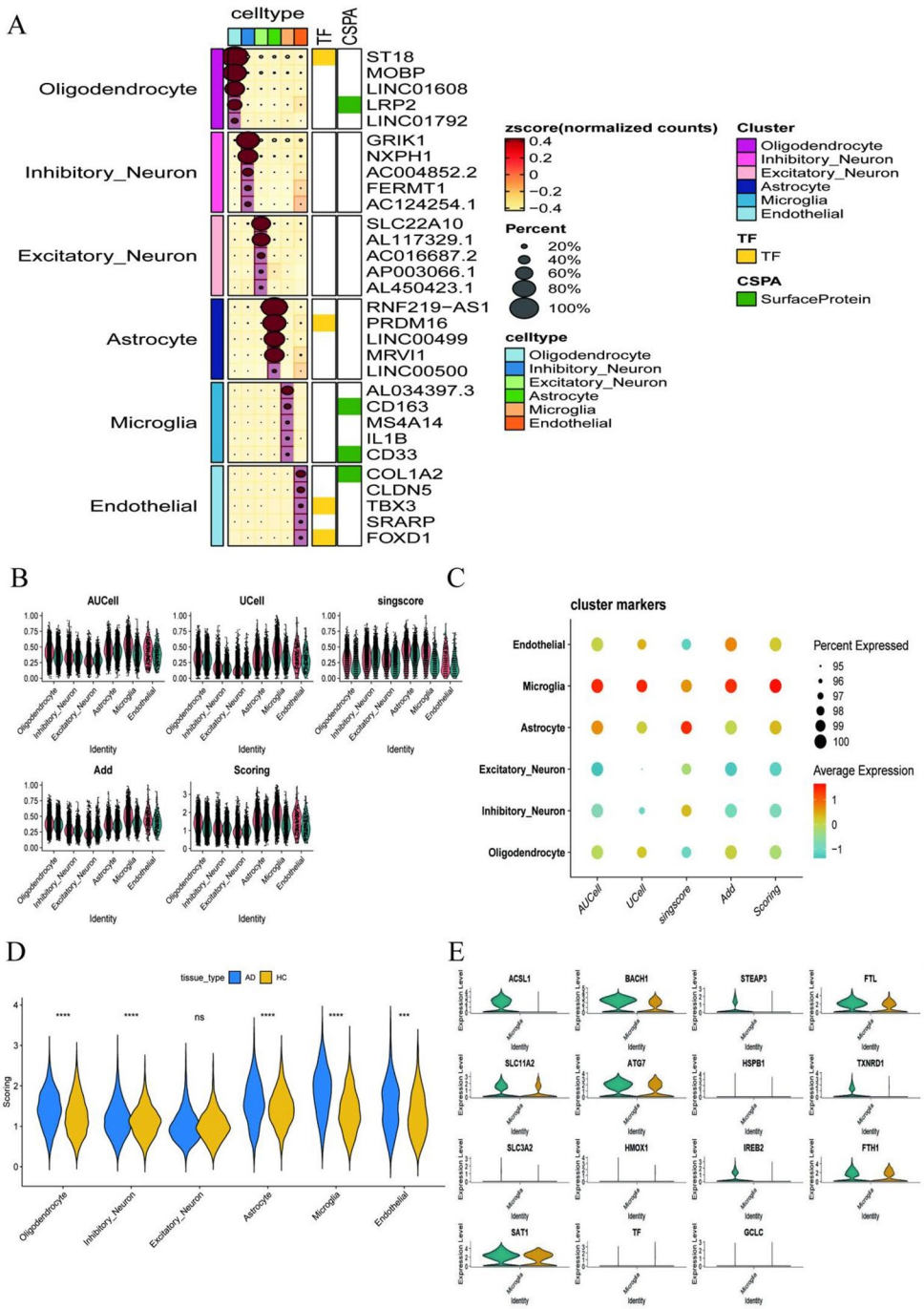

Fig. 2 Characterization of cell type-specific markers and functional signatures. (**A**) Heatmap and dot plot showing the expression profiles of canonical marker genes across the seven major cell lineages. The heatmap displays z-score normalized expression levels, while the adjacent dot plot indicates the percentage of cells expressing each gene (dot size) and the average expression level (color intensity). This confirms the distinct identity of each cell cluster, with specific markers such asMOBP for Oligodendrocytes, GAD1 for Inhibitory Neurons, SLC17A7 for Excitatory Neurons, AQP4 for Astrocytes, AIF1 for Microglia, andCLDN5 for Endothelial cells. (**B**) Violin plots illustrating the distribution of functional module scores (calculated using methods such as AUCell, UCell, or singscore) across different cell types. The scores reflect the enrichment of specific biological pathways or gene sets, revealing functional heterogeneity among the cell populations. (**C**) Dot plot summarizing the expression specificity of key cluster markers. The size of the dots represents the percentage of cells expressing the gene within each cluster, and the color scale indicates the average expression level, further validating the cell type annotation. (**D**) Violin plots displaying the expression distribution of specific genes of interest across the seven major cell lineages. This highlights the cellular specificity of these genes, showing which cell types contribute most significantly to their expression. (**E**) [Note: Since panel E is partially visible/cut off in the provided image, a general description is provided based on typical single-cell analysis figures]. Feature plots or violin plots showing the expression patterns of additional specific genes across the UMAP embedding or cell types, further detailing the molecular characteristics of the identified subpopulations

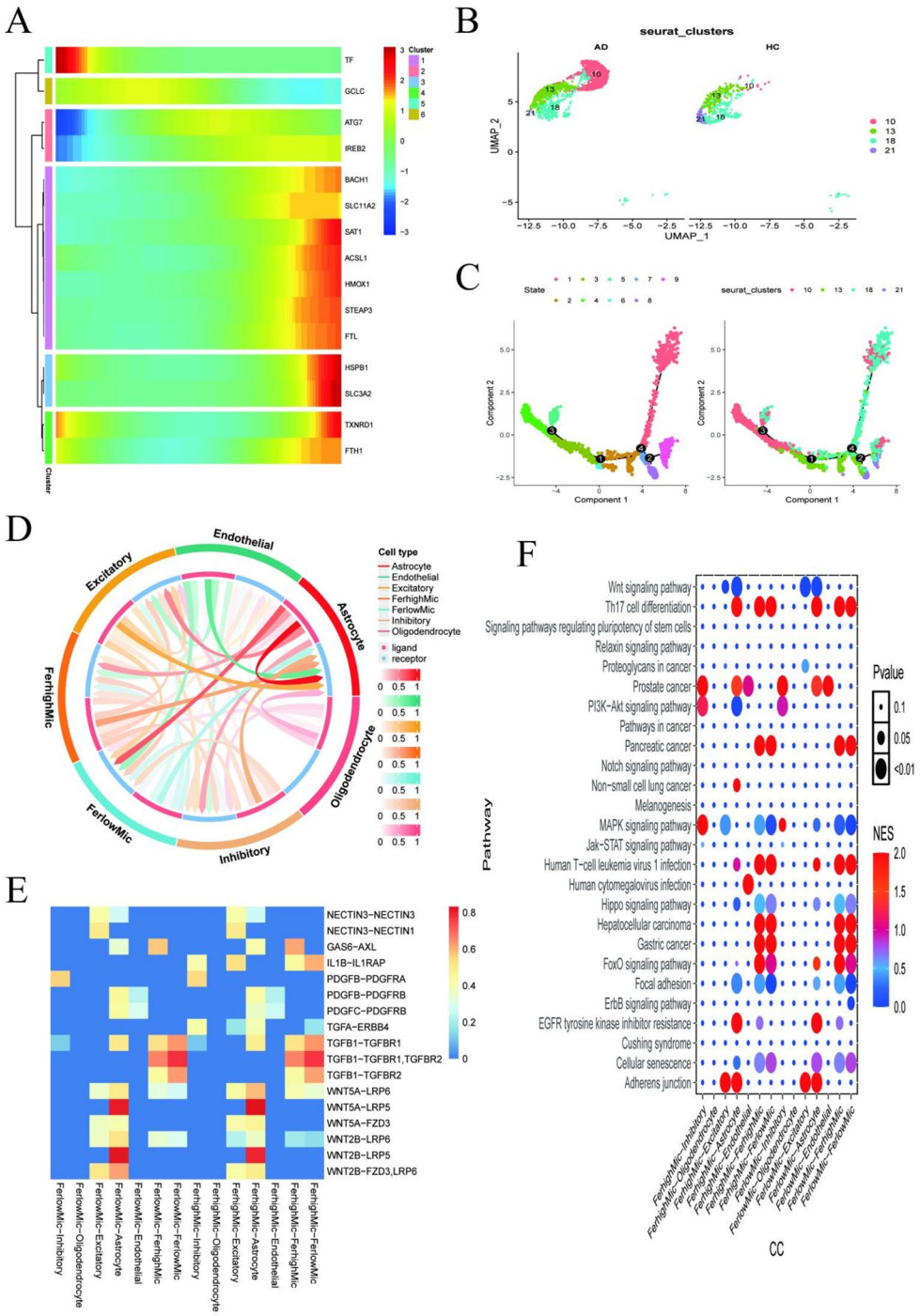

Fig. 3 Cellular interactions and dynamics of signaling pathways in disease vs. control cohorts. (**A**) A color-scaled matrix of the relative strength of the intercellular communication among the different cell populations. The vertical and horizontal axes are the different cellular subtypes, while the color is the corresponding magnitude of the signaling interaction, the brighter the color, the more the communication is strong. (**B**) Two-dimensional UMAP visualizations of the spatial arrangement of the cellular clusters, with a different color code between AD and healthy control (HC) samples. (**C**) UMAP projections of the expression of the particular gene sets among the different cellular subgroups, the color gradients indicate the degree of module activation. (**D**) A circular diagram of the web of signaling exchanges between the principal cellular lineages. The thickness of the connecting bands is the interaction intensity, and the chromatic variation identify the participating cell types, showing the network of molecular communication. (**E**) A color-scaled matrix of the activation level of multiple biological signaling cascades among the different cellular populations. The visualization shows the intercellular communication in the form of different kinds of graphs. In the heatmap (**F**) horizontal axes represent different cellular populations and vertical axes show the molecular interaction networks of the NECTIN-NECTIN and CADM1-CADM. The colours gradation shows the magnitude of the pathway that is activated, the more vibrant the colour the more is the intensity of the signaling

ferroptosis related gene patterns. We found five clear cellular subgroups (Fig. 5A). The IREB2 positive MC C1 cluster (in red) had higher expression of iron regulation related genes, while the ACSB1 positive MC C3 cluster (in green) had a big enrichment of genes related to fatty acid metabolic processes.

In particular, the IREB2^{+} C1 cell group had a different inflammatory profile. Pathway enrichment study (Fig. 5B) shows that this subset is strongly involved in the Toll-like receptor cascades, IL-17 mediated signaling and atherosclerotic lipid metabolism pathway. Assessment of intercellular communication (Fig. 5C) shows that IREB2^{+} C1 is a

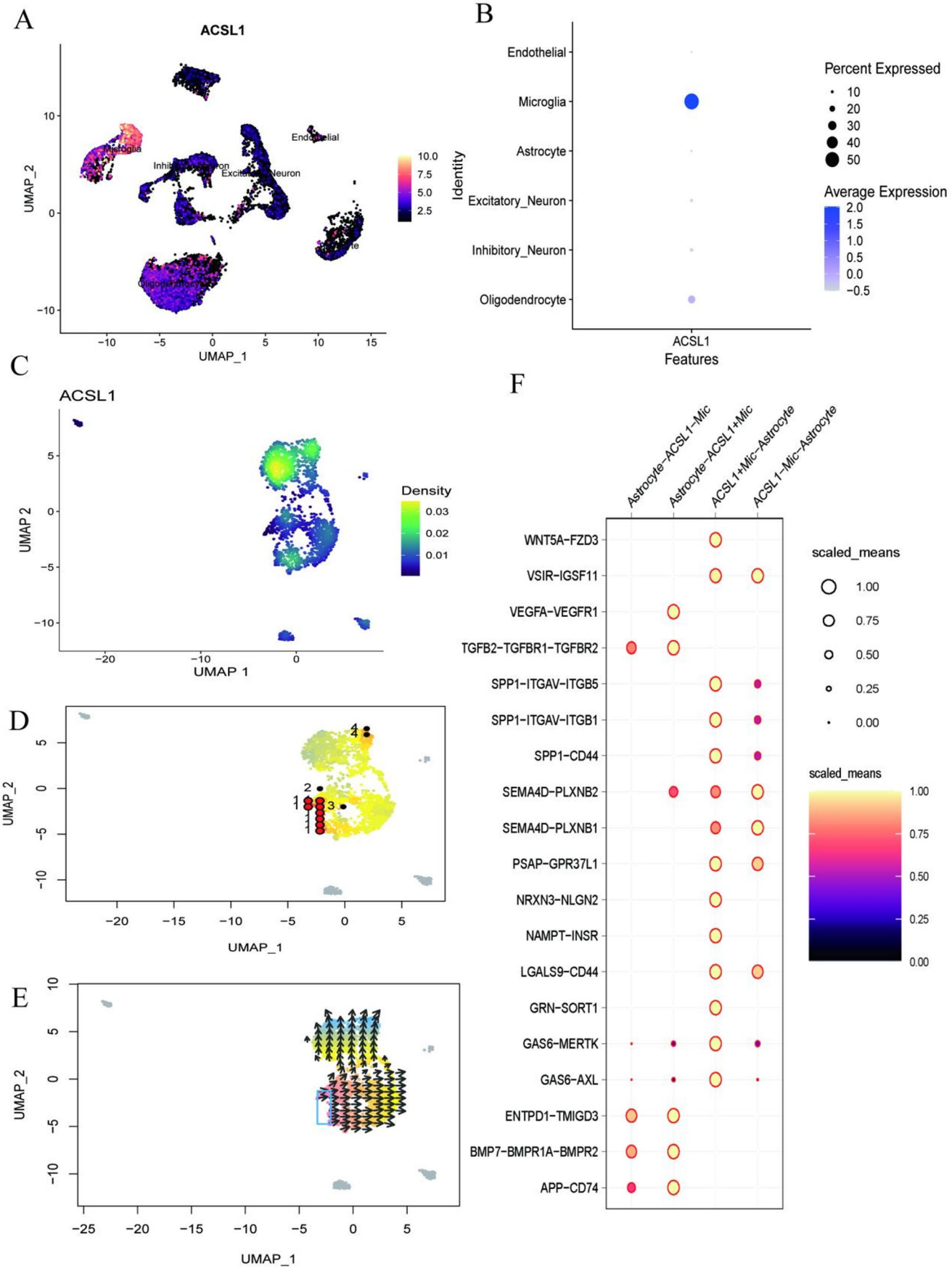
A
ACSL1
UMAP_2
UMAP_1
Endothelial
Microglia
Astrocyte
Excitatory_Neuron
Inhibitory_Neuron
Oligodendrocyte
10.0
7.5
5.0
2.5
B
Endothelial
Microglia
Astrocyte
Excitatory_Neuron
Inhibitory_Neuron
Oligodendrocyte
Identity
ACSL1
Features
Percent Expressed
10
20
30
40
50
Average Expression
2.0
1.5
1.0
0.5
0.0
−0.5
C
ACSL1
UMAP 2
UMAP 1
Density
0.03
0.02
0.01
D
UMAP_2
UMAP_1
E
UMAP_2
UMAP_1
F
Astrocyte−ACSL1−Mic
Astrocyte−ACSL1+Mic
ACSL1+Mic−Astrocyte
ACSL1−Mic−Astrocyte
WNT5A−FZD3
VSIR−IGSF11
VEGFA−VEGFR1
TGFB2−TGFBR1−TGFBR2
SPP1−ITGAV−ITGB5
SPP1−ITGAV−ITGB1
SPP1−CD44
SEMA4D−PLXNB2
SEMA4D−PLXNB1
PSAP−GPR37L1
NRXN3−NLGN2
NAMPT−INSR
LGALS9−CD44
GRN−SORT1
GAS6−MERTK
GAS6−AXL
ENTPD1−TMIGD3
BMP7−BMPR1A−BMPR2
APP−CD74
scaled_means
1.00
0.75
0.50
0.25
0.00
scaled_means
1.00
0.75
0.50
0.25
0.00

Fig. 4 Characterization of ACSL1 expression and its potential ligand-receptor interactions in the brain cellular landscape. (**A**) UMAP plot showing the expression level of ACSL1 across all cell types. The color scale represents the normalized expression level, indicating that ACSL1 is predominantly expressed in Oligodendrocytes and Microglia. (**B**) Dot plot summarizing ACSL1 expression across the seven major cell lineages. The dot size represents the percentage of cells expressing the gene, while the color intensity indicates the average expression level. This confirms the high and specific expression of ACSL1 in Oligodendrocytes and Microglia. (**C**) UMAP plot highlighting the density of cells with high ACSL1 expression. The color gradient from blue to yellow represents increasing cell density, further pinpointing the specific subpopulations within Oligodendrocytes and Microglia that are characterized by high ACSL1 levels. (**D**, **E**) UMAP plots visualizing the spatial distribution of specific cell clusters (labeled 0–15) identified within the ACSL1-high populations. These plots show the segregation of these cells into distinct subgroups. (**F**) Dot plot predicting potential ligand-receptor interactions associated with ACSL1 in Astrocytes and Microglia. The plot displays interactions for both ACSL1-high and ACSL1-low states. The circle size represents the scaled mean expression of the interaction pair, and the color indicates the interaction significance or strength. Notable interactions include SPP1-ITGAV-ITGB5 and GAS6-AXL, suggesting a role for ACSL1 in mediating cell-cell communication, particularly in phagocytic or inflammatory pathways

main source of signaling, with strong outgoing communication pattern, which means that this cell is in the center of the signaling of the inflammatory message in the brain affected by the Alzheimer's disease. Finally, the metabolic profiling (Fig. 5H and L) show that both IREB2$^+$ C1 and ACSB1$^+$ C3 population show strong activity in oxidative phosphorylation and glycolytic process, which suggest that the abnormalities in the iron metabolism are linked with the generation of energy which are sustained the inflammatory response.

Functional validation: IREB2 upregulation drives pro-inflammatory cytokine secretion

In order to test if the IREB2 molecular signature is causally related to the neuroinflammatory processes, we performed genetic manipulation experiments in SH-SY5Y and BV2 cell lines. Quantitative reverse transcription polymerase chain reaction analysis confirmed effective IREB2 gene overexpression after the transfection (Fig. 6A, E). As we observed in the single-cell RNA sequencing, the higher IREB2 expression strongly enhanced the inflammatory reaction. By enzyme-linked immunosorbent assay measurements, we saw a clear elevation in the release of the major inflammatory mediators, Interleukin-1- (Fig. 6B), Interleukin-6 (Fig. 6C), and Tumor necrosis factor- (Fig. 6D), in comparison with the cells that were not treated. These experimental results show that simply an increased expression of IREB2 is enough for inducing an inflammatory cellular state in the neuronal models. They provide solid evidence that links the iron homeostasis disruption found in the IREB2-positive macrophage subsets with the continuous neuroinflammation of the Alzheimer pathology, making IREB2 a key modulator in the inflammatory cascade of the disease.

Discussion

In this study, we used single-cell RNA-sequencing combined with non-negative matrix factorization (NMF) and cell-cell communication analysis to characterize a novel IREB2-expressing macrophage/microglial population in Alzheimer's disease (AD) brain tissues. We found a marked expansion of this cluster, which we termed IREB2$^+$ MC C1, in AD samples. Its transcriptional signature involves well-established inflammasome-related pathways, including Toll-like receptor signaling, IL-17-mediated responses, and complement system activation. These molecular patterns suggest that IREB2-expressing cells actively contribute to the persistent neuroinflammatory state in AD through multiple inflammatory cascades. This subset also exhibited the strongest outgoing signal transmission, indicating that it not only mediates inflammatory responses but also serves as a key initiator of intercellular communication. The microenvironment showed increased inflammatory signaling, and IREB2$^+$ MC C1 cells produced high levels of chemotactic cytokines (CCL3, CCL4) and immunomodulatory factors (SPP1, SEMA4D), which may recruit circulating immune cells and stimulate resident glia via paracrine mechanisms, further amplifying the inflammatory cascade.

We also identified a direct association between IREB2 expression and oxidative stress-related genes (SAT1, HSP90). This implies that IREB2 could promote reactive oxygen species production by regulating intracellular iron balance, thereby sustaining pro-inflammatory pathways. In this context, ACSL1 (acyl-CoA synthetase long-chain family member 1) — a key enzyme involved in lipid metabolism — was co-expressed with IREB2 in the same subpopulation. The concurrent upregulation of IREB2 and ACSL1 suggests a potential link between iron regulation, lipid metabolism, and neuroinflammation in AD.To test the causal role of IREB2 in AD-associated inflammation, we performed functional assays. scRNA-seq data revealed a strong positive correlation between IREB2 levels and multiple inflammatory genes (IL1B, TNF, CXCL10). Knockdown of endogenous IREB2 using specific siRNA markedly reduced the constitutive production of these mediators. Thus, IREB2

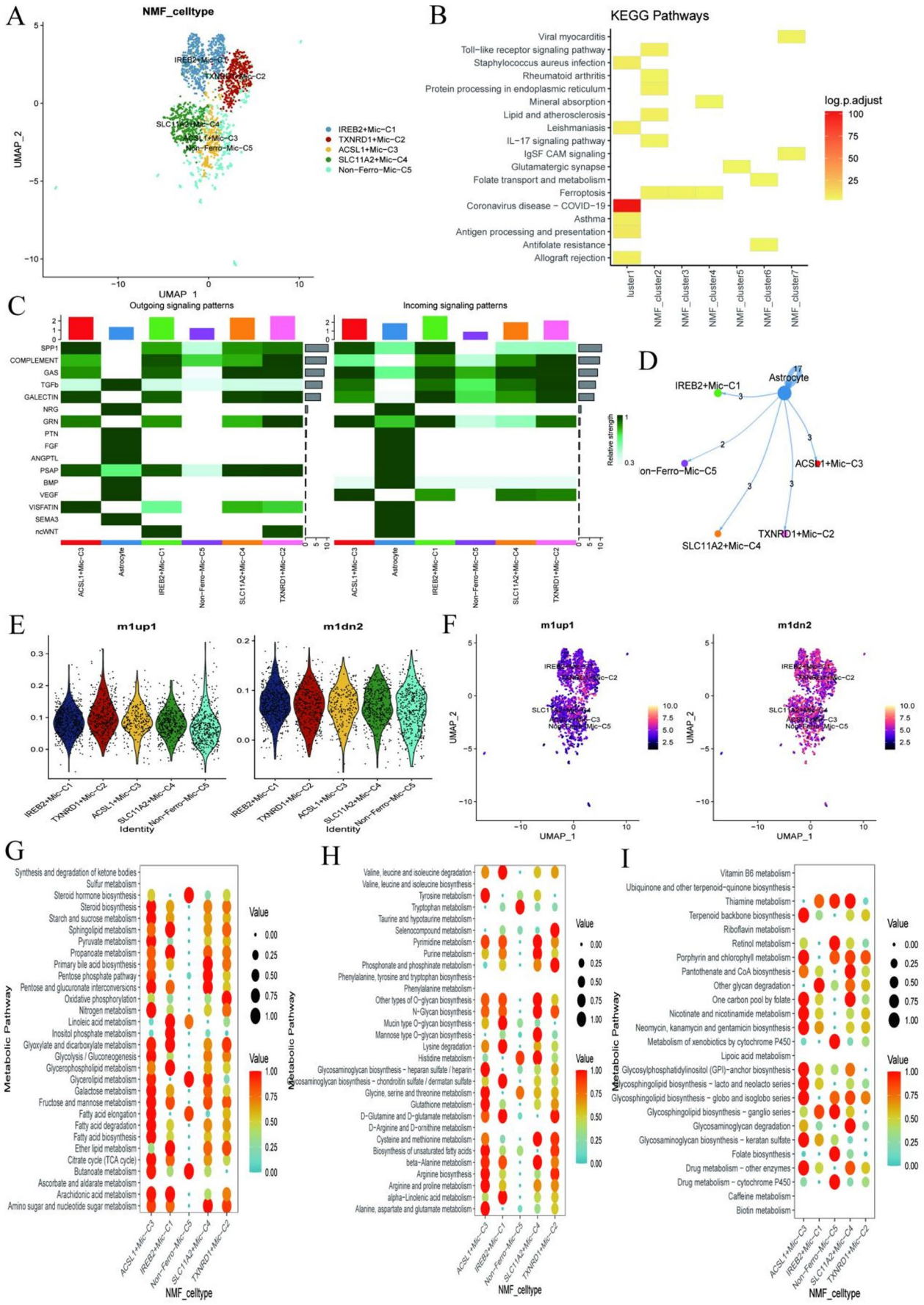
A
NMF_celltype
UMAP_1
UMAP_2
IREB2+Mic−C1
TXNRD1+Mic−C2
ACSL1+Mic−C3
SLC11A2+Mic−C4
Non−Ferro−Mic−C5
B
KEGG Pathways
Viral myocarditis
Toll−like receptor signaling pathway
Staphylococcus aureus infection
Rheumatoid arthritis
Protein processing in endoplasmic reticulum
Mineral absorption
Lipid and atherosclerosis
Leishmaniasis
IL−17 signaling pathway
IgSF CAM signaling
Glutamatergic synapse
Folate transport and metabolism
Ferroptosis
Coronavirus disease − COVID−19
Asthma
Antigen processing and presentation
Antifolate resistance
Allograft rejection
log.p.adjust
100
75
50
25
luster1
NMF_cluster2
NMF_cluster3
NMF_cluster4
NMF_cluster5
NMF_cluster6
NMF_cluster7
C
Outgoing signaling patterns
Incoming signaling patterns
SPP1
COMPLEMENT
GAS
TGFb
GALECTIN
NRG
GRN
PTN
FGF
ANGPTL
PSAP
BMP
VEGF
VISFATIN
SEMA3
ncWNT
ACSL1+Mic−C3
Astrocyte
IREB2+Mic−C1
Non−Ferro−Mic−C5
SLC11A2+Mic−C4
TXNRD1+Mic−C2
D
Astrocyte
IREB2+Mic−C1
ACSL1+Mic−C3
on−Ferro−Mic−C5
TXNRD1+Mic−C2
SLC11A2+Mic−C4
Relative strength
E
m1up1
m1dn2
Identity
F
m1up1
m1dn2
UMAP_1
UMAP_2
G
Synthesis and degradation of ketone bodies
Sulfur metabolism
Steroid hormone biosynthesis
Steroid biosynthesis
Starch and sucrose metabolism
Sphingolipid metabolism
Pyruvate metabolism
Propanoate metabolism
Primary bile acid biosynthesis
Pentose phosphate pathway
Pentose and glucuronate interconversions
Oxidative phosphorylation
Nitrogen metabolism
Linoleic acid metabolism
Inositol phosphate metabolism
Glyoxylate and dicarboxylate metabolism
Glycolysis / Gluconeogenesis
Glycerophospholipid metabolism
Glycerolipid metabolism
Galactose metabolism
Fructose and mannose metabolism
Fatty acid elongation
Fatty acid degradation
Fatty acid biosynthesis
Ether lipid metabolism
Citrate cycle (TCA cycle)
Butanoate metabolism
Ascorbate and aldarate metabolism
Arachidonic acid metabolism
Amino sugar and nucleotide sugar metabolism
Metabolic Pathway
NMF_celltype
Value
H
Valine, leucine and isoleucine degradation
Valine, leucine and isoleucine biosynthesis
Tyrosine metabolism
Tryptophan metabolism
Taurine and hypotaurine metabolism
Selenocompound metabolism
Pyrimidine metabolism
Purine metabolism
Phosphonate and phosphinate metabolism
Phenylalanine, tyrosine and tryptophan biosynthesis
Phenylalanine metabolism
Other types of O−glycan biosynthesis
N−Glycan biosynthesis
Mucin type O−glycan biosynthesis
Mannose type O−glycan biosynthesis
Lysine degradation
Histidine metabolism
Glycosaminoglycan biosynthesis − heparan sulfate / heparin
Glycosaminoglycan biosynthesis − chondroitin sulfate / dermatan sulfate
Glycine, serine and threonine metabolism
Glutathione metabolism
D−Glutamine and D−glutamate metabolism
D−Arginine and D−ornithine metabolism
Cysteine and methionine metabolism
Biosynthesis of unsaturated fatty acids
beta−Alanine metabolism
Arginine biosynthesis
Arginine and proline metabolism
alpha−Linolenic acid metabolism
Alanine, aspartate and glutamate metabolism
I
Vitamin B6 metabolism
Ubiquinone and other terpenoid−quinone biosynthesis
Thiamine metabolism
Terpenoid backbone biosynthesis
Riboflavin metabolism
Retinol metabolism
Porphyrin and chlorophyll metabolism
Pantothenate and CoA biosynthesis
Other glycan degradation
One carbon pool by folate
Nicotinate and nicotinamide metabolism
Neomycin, kanamycin and gentamicin biosynthesis
Metabolism of xenobiotics by cytochrome P450
Lipoic acid metabolism
Glycosylphosphatidylinositol (GPI)−anchor biosynthesis
Glycosphingolipid biosynthesis − lacto and neolacto series
Glycosphingolipid biosynthesis − globo and isoglobo series
Glycosphingolipid biosynthesis − ganglio series
Glycosaminoglycan degradation
Glycosaminoglycan biosynthesis − keratan sulfate
Folate biosynthesis
Drug metabolism − other enzymes
Drug metabolism − cytochrome P450
Caffeine metabolism
Biotin metabolism

Fig. 5 Comprehensive characterization of non-neuronal cell populations reveals distinct metabolic and signaling profiles associated with disease states. (**A**) UMAP visualization of non-neuronal cell types (MNP_celltype). Cells are colored by cluster identity, identifying distinct populations including microglia (ACSL1-Micro-C1), oligodendrocytes (TSPAN18-Od-C2), and astrocytes (SLC11A0-As-C3), as well as non-fiber and fiber-associated cells. (**B**) Heatmap displaying the results of KEGG pathway enrichment analysis for each cell cluster. The color intensity represents the adjusted p-value (-log10), highlighting significantly enriched pathways such as "Antigen processing and presentation," "Lipid and atherosclerosis," and "MAPK signaling pathway" across different cell types. (**C**) Heatmaps illustrating the outgoing (left) and incoming (right) signaling patterns for each cell cluster. The color scale indicates the communication probability, revealing distinct communication roles; for instance, specific microglial and oligodendrocyte clusters show unique outgoing and incoming signaling profiles. (**D**) Ligand-receptor interaction network centered on ACSL1. The plot depicts the communication links between ACSL1-expressing cells (ACSL1-Micro-C1) and other cell types, mediated by specific ligand-receptor pairs such as APP-CD74 and TSPAN8-TNFRSF1B. (**E**) Violin plots showing the expression distribution of specific marker genes (em1up1, em1down2) across the identified cell clusters. This demonstrates the differential expression patterns that define each subpopulation. (**F**) UMAP plots showing the spatial distribution and expression levels of em1up1 (left) and em1down2 (right) across the entire cell landscape. The color gradient indicates the expression level, confirming the cluster-specific enrichment observed in the violin plots. (**G**) Metabolic pathways related to lipid and amino acid metabolism. (**H**) Metabolic pathways related to energy and nucleotide metabolism. (**I**) Metabolic pathways related to xenobiotic and cofactor metabolism

drives the neuroinflammatory reaction in microglial cells, and high IREB2 levels are sufficient to impose a pro-inflammatory shift.

In addition, this study also has certain limitations. SH-SY5Y is a human neuroblastoma cell line, widely used as a neuronal model for the study of chronic neurodegenerative disorders in Alzheimer's disease (AD), to simulate the gene expression and ligand-receptor activity of neurons under long-term pathological stimulation. Regarding the discussion of microglia, it stems from the core pathological feature of AD - the chronic neuroinflammation mediated by microglia, as well as the close intercellular communication between neurons and microglia. This study uses SH-SY5Y cells, not to replace microglia, but from the perspective of neurons, to predict the possible cross-cell signaling networks they may be involved in. However, as an immortalized cell line derived from tumors, SH-SY5Y lacks the aging characteristics, metabolic state, and true response to chronic stress of primary neurons, and cannot directly reflect the function of microglia.

Conclusion

In summary, we identified a distinct IREB2^{+} macrophage/microglial subpopulation in AD that drives neuroinflammation, potentially via the NF-κB pathway, and accelerates neurodegenerative processes. IREB2 knockdown strongly reduces pro-inflammatory cytokine production. The IREB2^{+} MC C1 subset thus represents both a potential biomarker for AD and a promising anti-inflammatory therapeutic target. The co-expression of IREB2 and ACSL1 suggests an unexplored axis linking iron metabolism, lipid metabolism, and neuroinflammation, warranting further investigation.

Author contributions The research study was conceived by Wenzheng Rong, Jing Xu, Bo Li, Yapeng Li andYuming Xu. The manuscript was written by Wenzheng Rong, Jing Xu, Yapeng Li and Yuming Xu. The data collection and literature review was done by Wenzheng Rong, and the experimental procedure was done by Bo Li. The data analysis and data visualization were done by Wenzheng Rong and Yapeng Li. The manuscript revision was help by Yuming Xu. All authors contributed to reviewing and approving the final version of the manuscript.

Funding The National Natural Science Foundation of China [Grant U1904207], National Key R&D Program of China [Grant 2017YFA0105003], Non-profit Central Research Institute Fund of Chinese Academy of Medical Sciences [Grant 2020-PT310-01], and

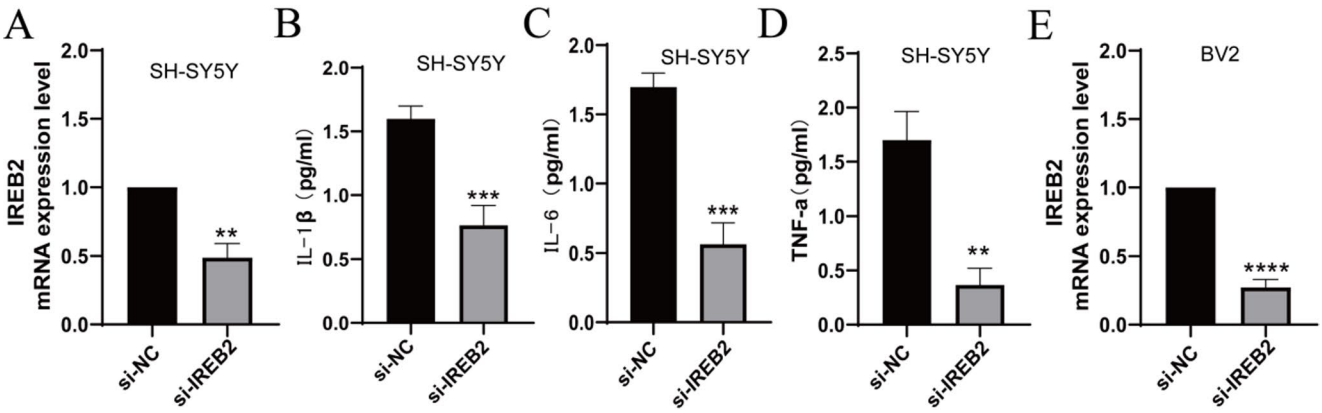

Fig. 6 Effect of IREB2 knockdown on inflammatory cytokine secretion in SH-SY5Y cells. (**A**,**E**) IREB2 mRNA expression levels were measured by qRT-PCR in SH-SY5Y and BV2 cells transfected with negative control siRNA (si-NC) or IREB2-targeting siRNA (si-IREB2). (**B**-**D**) The protein concentrations of IL-1β (B), IL-6 (**C**), and TNF-α (**D**) in the cell culture supernatants were determined by ELISA.Data are presented as mean ± SD. $^{**}P<0.01$, $^{***}P<0.001$ vs. si-NC group

Innovative and Scientific and Technological Talents Training Project of Henan Province [Grant YXKC2021062] all provided funding for this work.

Data availability No datasets were generated or analysed during the current study.

Declarations

Competing interests The authors declare no competing interests.

References

1. Se Thoe E, Fauzi A, Tang YQ, Chamyuang S, Chia AYY. A review on advances of treatment modalities for Alzheimer's disease. Life Sci. 2021;276:119129.
2. Zhang D, Zhang W, Ming C, Gao X, Yuan H, Lin X, et al. P-tau217 correlates with neurodegeneration in Alzheimer's disease, and targeting p-tau217 with immunotherapy ameliorates murine tauopathy. Neuron. 2024;112(10):1676–e169312.
3. Angelucci F, Cechova K, Amlerova J, Hort J. Antibiotics, gut microbiota, and Alzheimer's disease. J Neuroinflammation. 2019;16(1):108.
4. Zhang P, Kishimoto Y, Grammatikakis I, Gottimukkala K, Cutler RG, Zhang S, et al. Senolytic therapy alleviates Aβ-associated oligodendrocyte progenitor cell senescence and cognitive deficits in an Alzheimer's disease model. Nat Neurosci. 2019;22(5):719–28.
5. Peng D, Liu T, Lu H, Zhang L, Chen H, Huang Y, et al. Intranasal delivery of engineered extracellular vesicles loaded with miR-206-3p antagomir ameliorates Alzheimer's disease phenotypes. Theranostics. 2024;14(19):7623–44.
6. Wang C, Zong S, Cui X, Wang X, Wu S, Wang L, et al. The effects of microglia-associated neuroinflammation on Alzheimer's disease. Front Immunol. 2023;14:1117172.
7. Wang M, Zhang H, Liang J, Huang J, Chen N. Exercise suppresses neuroinflammation for alleviating Alzheimer's disease. J Neuroinflammation. 2023;20(1):76.
8. Wang C, Chen S, Guo H, Jiang H, Liu H, Fu H, et al. Forsythoside A Mitigates Alzheimer's-like Pathology by Inhibiting Ferroptosis-mediated Neuroinflammation via Nrf2/GPX4 Axis Activation. Int J Biol Sci. 2022;18(5):2075–90.
9. Singh D. Astrocytic and microglial cells as the modulators of neuroinflammation in Alzheimer's disease. J Neuroinflammation. 2022;19(1):206.
10. Mangalmurti A, Lukens JR. How neurons die in Alzheimer's disease: Implications for neuroinflammation. Curr Opin Neurobiol. 2022;75:102575.
11. Green GS, Fujita M, Yang HS, Taga M, Cain A, McCabe C, et al. Cellular communities reveal trajectories of brain ageing and Alzheimer's disease. Nature. 2024;633(8030):634–45.
12. Gazestani V, Kamath T, Nadaf NM, Dougalis A, Burris SJ, Rooney B, et al. Early Alzheimer's disease pathology in human cortex involves transient cell states. Cell. 2023;186(20):4438–e445323.
13. Depp C, Sun T, Sasmita AO, Spieth L, Berghoff SA, Nazarenko T, et al. Myelin dysfunction drives amyloid-β deposition in models of Alzheimer's disease. Nature. 2023;618(7964):349–57.
14. Wang C, Acosta D, McNutt M, Bian J, Ma A, Fu H, et al. A single-cell and spatial RNA-seq database for Alzheimer's disease (ssREAD). Nat Commun. 2024;15(1):4710.
15. Zeng J, Zhang R, Xu H, Zhang C, Lu L. Integrative single-cell RNA sequencing and mendelian randomization analysis reveal the potential role of synaptic vesicle cycling-related genes in Alzheimer's disease. J Prev Alzheimers Dis. 2025;12(5):100097.
16. Bai R, Guo J, Ye XY, Xie Y, Xie T. Oxidative stress: The core pathogenesis and mechanism of Alzheimer's disease. Ageing Res Rev. 2022;77:101619.
17. D'Alessandro MCB, Kanaan S, Geller M, Praticò D, Daher JPL. Mitochondrial dysfunction in Alzheimer's disease. Ageing Res Rev. 2025;107:102713.
18. Guan L, Mao Z, Yang S, Wu G, Chen Y, Yin L, et al. Dioscin alleviates Alzheimer's disease through regulating RAGE/NOX4 mediated oxidative stress and inflammation. Biomed Pharmacother. 2022;152:113248.
19. Park MW, Cha HW, Kim J, Kim JH, Yang H, Yoon S, et al. NOX4 promotes ferroptosis of astrocytes by oxidative stress-induced lipid peroxidation via the impairment of mitochondrial metabolism in Alzheimer's diseases. Redox Biol. 2021;41:101947.
20. Peng Y, Yao SY, Chen Q, Jin H, Du MQ, Xue YH, et al. True or false? Alzheimer's disease is type 3 diabetes: Evidences from bench to bedside. Ageing Res Rev. 2024;99:102383.
21. Sun C, Gao X, Sha S, Wang S, Shan Y, Li L, et al. Berberine alleviates Alzheimer's disease by activating autophagy and inhibiting ferroptosis through the JNK-p38MAPK signaling pathway. Int Immunopharmacol. 2025;155:114550.
22. Ma F, Wang L, Chi H, Li X, Xu Y, Chen K, et al. Exploring the Therapeutic Potential of MIR-140-3p in Osteoarthritis: Targeting CILP and Ferroptosis for Novel Treatment Strategies. Cell Prolif. 2025;58(11):e70018.
23. Jiang L, Jiang Y, Zhou X, Wang L, Zhang S, Jiang C, et al. The Key Role of COA6 in Pancreatic Ductal Adenocarcinoma: Metabolic Reprogramming and Regulation of the Immune Microenvironment. J Cell Mol Med. 2025;29(13):e70685.
24. Zhang P, Wang L, Liu H, Lin S, Guo D. Unveiling the crucial role of glycosylation modification in lung adenocarcinoma metastasis through artificial neural network-based spatial multi-omics single-cell analysis and Mendelian randomization. BMC Cancer. 2025;25(1):249.
25. Zhang P, Wang L, Lin H, Han Y, Zhou J, Song H, et al. Integrative multiomics analysis reveals the subtypes and key mechanisms of platinum resistance in gastric cancer: identification of KLF9 as a promising therapeutic target. J Transl Med. 2025;23(1):877.